J Mater Sci: Mater Med (2016) 27:52
DOI 10.1007/s10856-015-5661-6

Osteogenic response and osteoprotective effects in vivo of a nanostructured titanium surface with antibacterial properties

F. Ravanetti[1] · R. Chiesa[2] · M. C. Ossiprandi[1] · F. Gazza[1] · V. Farina[3] · F. M. Martini[1] · R. Di Lecce[1] · G. Gnudi[1] · C. Della Valle[2] · J. Gavini[1] · A. Cacchioli[1]

Received: 15 July 2015 / Accepted: 28 December 2015 / Published online: 19 January 2016

Abstract In implantology, as an alternative approach to the use of antibiotics, direct surface modifications of the implant addressed to inhibit bacterial adhesion and to limit bacterial proliferation are a promising tactic. The present study evaluates in an in vivo normal model the osteogenic response and the osteointegration of an anodic spark deposition nanostructured titanium surface doped with gallium (ASD + Ga) in comparison with two other surface treatments of titanium: an anodic spark deposition treatment without gallium (ASD) and an acid etching treatment (CTR). Moreover the study assesses the osteoprotective potential and the antibacterial effect of the previously mentioned surface treatments in an experimentally-induced peri-implantitis model. The obtained data points out a more rapid primary fixation in ASD and ASD + Ga implants, compared with CTR surface. Regarding the antibacterial properties, the ASD + Ga surface shows osteoprotective action on bone peri-implant tissue in vivo as well as an antibacterial effect within the first considered time point.

Electronic supplementary material The online version of this article (doi:10.1007/s10856-015-5661-6) contains supplementary material, which is available to authorized users.

✉ F. Ravanetti
francesca.ravanetti@unipr.it

[1] Department of Veterinary Science, University of Parma, Via del Taglio 10, 43126 Parma, Italy

[2] Department of Chemistry, Materials and Materials Engineering "G. Natta", Politecnico di Milano, Via Mancinelli 7, 20131 Milan, Italy

[3] Department of Veterinary Medicine, University of Sassari, Via Vienna 2, 07100 Sassari, Italy

Graphical Abstract

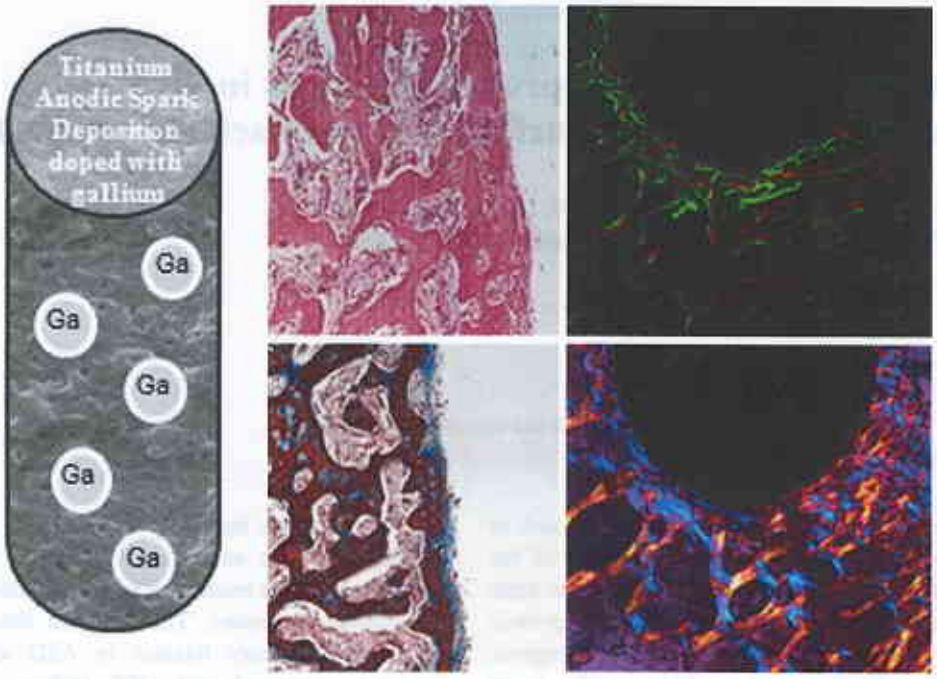

1 Introduction

In implantology, the surgical site infection (SSI) is an infection that occurs within one year after operation and appears to be related to the surgery [1]. The postoperative SSI represents an intrinsic risk of any surgical procedures, but when the surgery includes the implant of a biomaterial also the challenge of biomaterial related infections arises [2]. The fate on available surface may be conceptualized as a race for the surface, which is a contest between tissue cells integration and bacterial adhesion for dominance of the implant surface [3]. Bacterial adhesion to biomaterial surfaces is the essential step in the pathogenesis of infections and depends mainly on the superficial topography and chemical nature of the implanted materials [4]. In prosthetic implants, it is to consider that the bone to material interface represent a region of local immune depression. In addition, the micromovements and the release of wear debris in endosseous implants, as in the case of total orthoprosthesis, can damage the tissues surrounding the implant inducing a depletion of immune defense [5, 6]. Regarding the endosseous implant-related infections, the main etiological agent, both in human and in veterinary medicine, is *Staphylococcus aureus*, that causes the 34–50 % of total infections [7–9]. In this field, the research is developing complementary strategies to the use of systemic antibiotics such as local drug delivery systems that recently have achieved great attention to both infection prophylaxis and treatment. The local antibiotics delivery systems such as loaded bone cement [10, 11], loaded collagen sponge [12, 13] and loaded demineralized bone matrix [14] ensure greater durability and concentration in situ, regardless of vascular distribution [15]. Considering the problem of the increasing incidence of multidrug resistant implant infections [5, 16], the research is developing alternative approaches to the use of antibiotics, which are based on the direct modification of the implant surface with the aim to inhibit bacterial adhesion and limit bacterial proliferation [17, 18]. In order to obtain physico-chemical surface modification some treatments were developed using surfactants, proteins (such as albumin), polysaccharides (such as chitosan and hyaluronic acid), hydrophilic negatively-charged polysaccharides (such as hyaluronan and heparin) and light irradiation [19–21]. Another strategy is the use of anti-adhesive polymer coatings on titanium such as the hydrophilic poly (methacrylic acid) [22] and protein-resistant poly(ethylene glycol) [23]. One of the most promising strategies currently available for creating antibacterial coatings for titanium is the incorporation of metallic antibacterial agents directly on the titanium oxide layer [24, 25]. Inorganic antimicrobial agents mainly silver and copper were found very attractive for the doping of biomaterials because they possess many advantages such as good antibacterial ability,

excellent biocompatibility, and satisfactory stability [25–29]. Despite numerous studies were performed in this regard, the safety of silver remains a controversial topic [30]. More recently, gallium, a semi-metallic element in group 13 (IIIa) of the periodic table, showed efficacy in the treatment of several diverse disorders including the treatment of infections [31–34]. The solution and coordination chemistries of Ga^{3+} are very similar to those of Fe^{3+}. Due to the chemical similarities of Ga^{3+} with Fe^{3+} in terms of charge, ionic radius, electronic configuration and coordination number, gallium can substitute for iron in many biological systems [35]. In fact, gallium can replace iron in terms of antibacterial activity but at the same time its irreducibility alters the intracellular metabolic processes of prokaryotic cells, without inducing toxicity in eukaryotic cells. In fact, as to the mechanism of action of its antibacterial activity gallium replaces iron but its irreducibility alters the intracellular metabolic processes of prokaryotic cells, without inducing toxicity to eukaryotic cells. Precisely, in bone biology, an interesting feature of gallium is to present anti-resorptive effect as it blocks the osteoclastic related resorption process [36, 37].

One essential requirement for all antibacterial treatments is that they should not interfere with the tissue-integration. Indeed, if the tissue achieves quickly a good integration with the implant, the implant surface is also less available for bacterial colonization. The aim of the present study is primarily to evaluate in a normal model the osteogenic response and the osteointegration of an anodic spark deposition nanostructured titanium surface doped with gallium (ASD + Ga) in comparison with two other surface treatments of titanium: an anodic spark deposition treatment without gallium (ASD) and an acid etching treatment (CTR). The second purpose of the study is to assess the osteoprotective potential and the antibacterial effect of the previously mentioned surface treatments in an experimentally-induced peri-implantitis model. To do this we used peri-implantitis model [38] and two close time points (one and 2 weeks), in order to have a model aggressive enough to shortly develop peri-implantitis necessary to evaluate the behavior of gallium during primary bone fixation and infection, and at the same time protect the dignity and welfare of animals.

2 Materials and methods

2.1 Titanium implants preparation

All titanium samples used in this work were obtained from commercially pure, grade 2 biomedical grade (ISO 5832-2) titanium. Cylindrical implant samples (3 mm diameter, 13 mm length) were machined from titanium bars. Three different surface treatments (for detailed methods of implants preparation view the Supporting information) were considered and tested:

- CTR (acid-etched titanium);
- ASD (anodic spark deposition nanostructured titanium surface);
- ADS + Ga (anodic spark deposition nanostructured titanium surface doped with gallium).

Before undergoing any treatments, all titanium specimens were cleaned by ultrasonic rinsing (Elma Elmasonic S 60/H, Germany) in acetone (RPE Carlo Erba, Italy) for 10 min, then rinsed in Millipore water for 10 min. Finally, the specimens were dried in a thermostatic oven at 37 °C for 2 h. CRT treatment consisted in a double step chemical etching, the first carried out in a solution of 1 M NaOH with 2 % v/v H2O2, at 80 °C for 10 min; the second, after three washes in distilled water by ultrasonic rinsing, performed in a proper acid solution, kept at 50 °C for 30 min, capable to removing the protective passivation titanium oxide layer and to slowly erode titanium. ASD and ASD + Ga treatments were performed using a programmable DC power supply (N5772A, Agilent Technologies, Everett, WA, USA) in galvano-static conditions until reaching the final potential of 295 V for ASD and 325 V for ASD + Ga, in two different electrolytic solutions, kept stirred by magnetic stirring. For ASD was used a solution containing 0.03 M di Na_2SiO_3* $2H_2O$; 0.1 M ß-GP, 0.3 M di $C_4H_6CaO_4$*H_2O, 0.036 M NaOH corresponding to the treatment SiB as described in [39] and EP2479318-A1 (2012) by Chiesa R, Cigada A, Della Valle C, Rondelli G, Candiani G, Giordano G: "Metal substrates modified with silicon-based biomimetic treatment for the osteointegration thereof". ASD + Ga treatment was performed in the same electrochemical conditions of ASD treatment, with a final voltage set at 325 V and with the electrochemical solution used for ASD additivated with 0.004 M of Gallium Nitrate (Sigma-Aldrich, 289892) and with 0.306 M of Oxalic Acid Dihydrate (Sigma-Aldrich, 75699) used as chelating agent.

The three different surface modification treatments were analyzed using scanning electron microscopy (ZEISS-EVO 50 EP and Cambridge—Stereoscan 360) to assess surface morphology, while electron dispersion spectroscopy analysis (EDS, Oxford, Inca Energy 200) was performed at 20 kV and 500× magnification to qualitatively assess the surface chemical composition.

2.2 Experimental plan

Twelve skeletally mature outbred male New Zealand white rabbits weighed 3.2 ± 0.2 kg were used. The experiment

(including pre-operative, operative and post-operative care and maintenance of the animals) was performed following the European and Italian regulations on animal experimentation, according to the European Commission rules (European Union 2010/63—Health Ministry Authorization 14/06/2013). Rabbits were checked daily, housed in separate cages (size: 67 × 60 × 35 cm), received commercial food (pellets) and water ad libitum. The study design is based on a bilateral approach and the anatomical site for the implant was the distal epiphysis of the femur. Surgery was performed in sterile conditions under general anesthesia (Domitor, Pfizer, 0.1 ml kg^{-1}; Ketavet 100, Gellini, 0.3 ml kg^{-1}; Isoflurane-Vet, Mérial). After arthrotomy and dislocation, the holes in the trochlear groove were prepared using a low rotational drilling speed up to a diameter of 3.00 mm and continuous internal cooling, parallel to the longitudinal axis of the femur. Rabbits were randomly divided in two groups: normal model (not infected—NI) and experimentally induced peri-implantitis model (infected—I). Animals of normal model (NI), were aseptically implanted, whereas in the animals of experimentally induced peri-implantitis models (I), each implant was inoculated with 10^5 CFU/mL of *S. aureus* (ATCC25923) for six minutes before the implant placement, as previously reported by Chai et al. [38]. A total of 24 implants, eight for each surface (ETC, ASD and ASD + Ga) were inserted into the left and right femoral epiphysis of the rabbits as a bilateral approach, avoiding implanting the same materials in the counter lateral. The experimental times of 1 week (T1) and 2 weeks (T2) were considered. To evaluate the osteogenic activity, two fluorochromic bone markers [40] were sequentially administered subcutaneously as follows: Calcein Green (CG) (5 mg kg^{-1} BW; Sigma) was administered on the fifth and 6th day after surgery to all animals (1 W and 2 W); Xylenol Orange (XO) (90 mg kg^{-1} BW; Sigma) was administered on the 12th and 13th day after surgery only to the 2 W animals. A sequential radiographic analysis was performed to verify the correct location of the implant, immediately after surgery (T0) and to evaluate the bony tissue adjacent to the implant, immediately after the sacrifice at 1 or 2 W. At the end of the experimental trials, rabbits were pharmacologically euthanized (Tanax, 0.3 ml kg^{-1}/BW) and the distal epiphysis of each femur containing implants was explanted in sterile conditions. After an incision through the trochlear groove, parallel to the longitudinal axis of the femur, two bone segments were obtained with a fracture technique: one having a preserved implant-bone interface, was used for resin embedding and histomorphometric evaluation, the other was used for paraffin embedding and histology.

2.3 Microbiological evaluation

Immediately after sampling, two swabs were taken aseptically for each implant: one from implant surface and the other one from interfacial tissue exposed along the implant site. The swabs were placed into mannitol salt agar (MSA) culture plates, which were incubated at 37° for 24 h. At the

Table 1 Histomorphometric results (mean ± SD) at T1 and T2 for the CTR, ASD and ASD + Ga surfaces in normal model (NI) and experimentally induced peri-implantitis model (I)

Times	Parameter	Model	Surface		
			CTR	ASD	ASD+Ga
T1	BIC (%)	NI	47.35 ± 13.90	67.51 ± 23.63	69.91 ± 13.30
		I	57.87 ± 18.00	70.53 ± 10.78	84.66 ± 7.26
	BV (%)	NI	35.47 ± 7.34	51.05 ± 13.43	51.53 ± 5.84
		I	33.51 ± 6.53	42.71 ± 11.17	43.70 ± 12.84
	MV-CG (%)	NI	25.86 ± 6.39	39.88 ± 14.69	46.2 ± 9.71
		I	10.44 ± 6.97	28.76 ± 9.74	55.67 ± 22.66
T2	BIC (%)	NI	56.50 ± 16.84	80.95 ± 8.75	75.32 ± 6.92
		I	47.57 ± 1.61	70.21 ± 14.09	87.00 ± 8.07
	BV (%)	NI	54.37 ± 13.51	69.49 ± 8.02	65.96 ± 4.85
		I	32.47 ± 5.50	42.84 ± 14.58	52.08 ± 9.47
	MV-CG (%)	NI	21.52 ± 9.88	14.00 ± 4.06	19.92 ± 4.74
		I	7.97 ± 1.79	12.91 ± 7.74	15.36 ± 9.41
	MV-XO (%)	NI	16.02 ± 9.39	15.79 ± 3.21	18.13 ± 5.12
		I	6.81 ± 0.93	6.88 ± 3.52	9.12 ± 6.11

Histomorphometric parameters: *BIC* bone–implant contact, *BV* bone volume; *MV-CG* mineralizing volume for the CG marker, *MV-XO* mineralizing volume for the XO marker

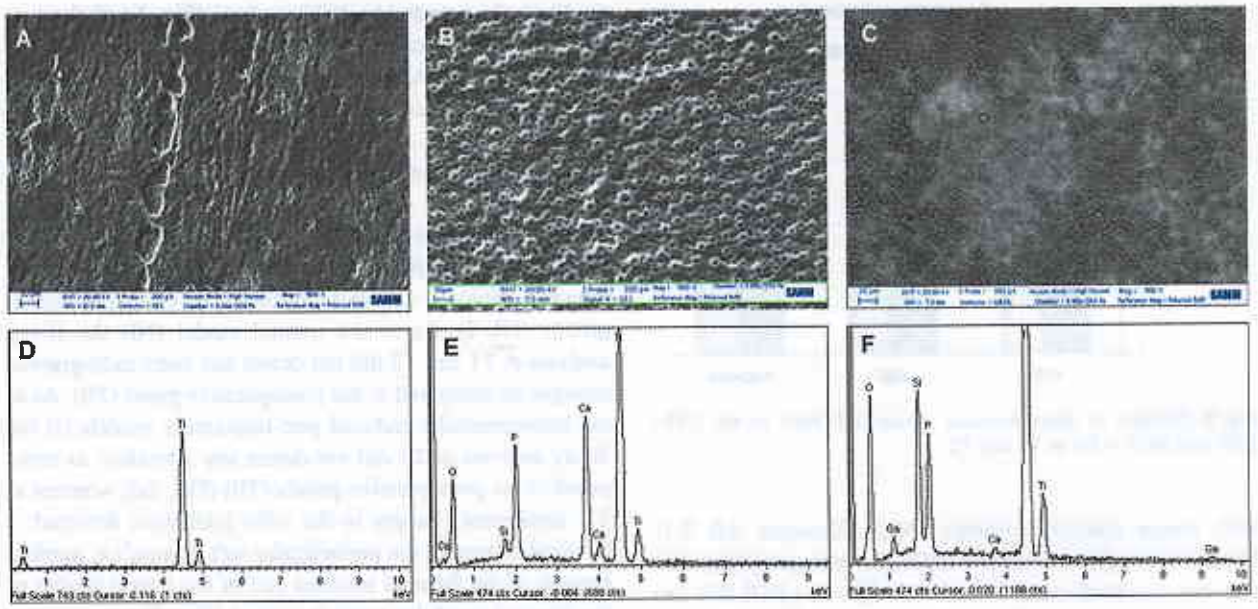

Fig. 1 Scanning Electron Microscopy of the surface morphology **a** ETC, **b** ASD and **c** ASD + Ga treatments and the respective EDS analysis of **d** ETC, **e** ASD and **f** ASD + Ga

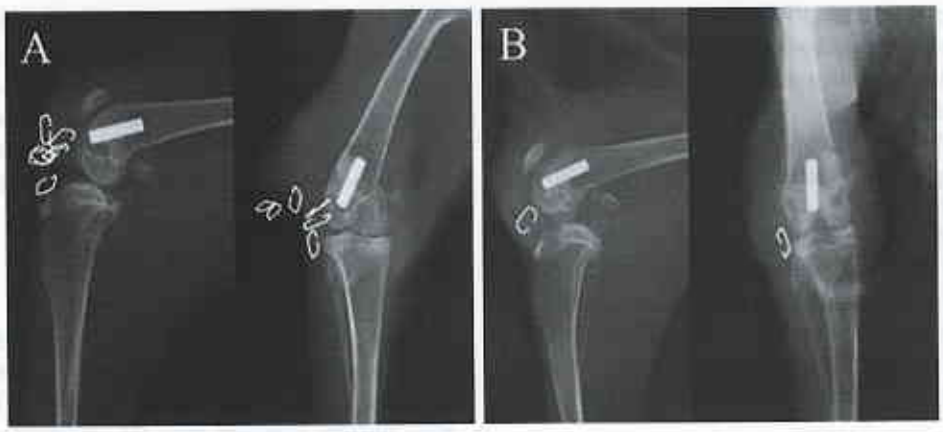

Fig. 2 X-ray analysis of experimentally induced peri-implantitis models at T1 (**a**) and T2 (**b**)

end of the incubation period, the number of CFUs was counted for each agar plate.

2.4 Histological and histomorphometric analysis

Bone samples were fixed in 4 % paraformaldehyde for 24 h. The bone samples with no implant, directed to histology, were decalcified in EDTA, dehydrated in graded alcohol solutions, xylene clarified and paraffin embedded. Serial section parallel serial to the bone longitudinal axis (5 μm thick) were obtained using a rotary microtome (Leica RM2155) and finally stained with hematoxylin-eosin, Masson's trichrome and Gram staining.

The bone segments containing implants, used for histomorphometric analysis, were dehydrated in graded alcohol solutions, xylene clarified, and polymethylmethacrylate resin embedded (Osteo-Bed, Polyscience). Non-decalcified perpendicular serial sections perpendicular to the bone longitudinal axis (50 μm thick), were obtained using a Leiz 1600 microtome (Leica). Histomorphometric analysis was performed at the magnification of 10× considering eight sections per sample. The sections were analyzed under polarized light microscopy for static histomorphometric analysis and under fluorescence microscopy for dynamic histomorphometric analysis by motorized microscope (Nikon Eclipse 90i), equipped with a digital camera (Nikon model 5 M) connected to a PC

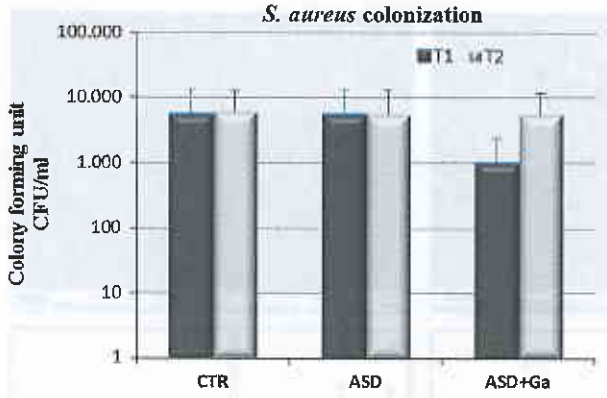

Fig. 3 Titration of *Staphylococcus aureus* (CFU/ml) on the CTR; ASD and ASD + Ga at T1 and T2

with image analysis software (NIS—Elements AR 2.1; Nikon). As region of Interest (ROI) the histomorphometric analysis was performed within an *half-crown* ROI 400 μm thick consecutive to the implant surface. The following static and dynamic histomorphometric parameters [41] were measured:

- Bone to implant contact (BIC) (%): it was calculated as the ratio between the length of the bone profile in direct contact with the implant surface and the length of the implant profile;
- Bone volume (BV) (%): it was calculated under polarized light as the ratio between the bone volume and the ROI volume.
- Mineralizing volume (MV) (%): it was calculated as the ratio between the surface marked with the vital marker and the bone surface within the ROI. This parameter was measured for each vital marker. For the CG marker (MV-CG) it was calculated in both T1 and T2, for the XO marker (MV-XO), it was calculated just within the T2.

Results are presented as mean ± standard deviation (Table 1). Data were analyzed with the analysis of variance (ANOVA) with Sidak correction. All analyses were performed with IBM SPSS statistics software v.21. The confidence level was set at 95 %.

3 Results

3.1 Morphological characterization

Figures 1a–c show SEM image of the surface morphology of ETC, ASD and ASD + Ga treatments respectively. ETC show a morphology typical of micro-etched surface. Both ASD and ASD + Ga show a morphology characterized by micrometric pores, bigger, more regular and homogeneous for ASD treatment. The surface chemical composition qualitatively detected by EDS analysis (Fig. 1d–f) show as expected pure titanium for ETC, while Si, Ca, and P where visible on ASD. ASD + Ga, besides Ca, Si and P detect also the presence of some Ga.

3.2 Radiological evaluation

The radiographic examination at T0 confirmed the correct location of the implants in the central portion of the distal femoral epiphysis and metaphysis of all the experimental groups (NI, I). As to the normal model (NI) the X-ray analysis at T1 and T2 did not detect any bony radiographic changes as compared to the postoperative panel (T0). As to the experimentally induced peri-implantitis models (I) the X-ray analysis at T1 did not detect any alteration as compared to the postoperative panels (T0) (Fig. 2a), whereas at T2, significant changes in the stifle joint were detected: a bilateral edema of the periarticular soft tissues, i.e. marked erosion of the femoral trochlea and of the lateral profile of the femoral condyles were described (Fig. 2b).

3.3 Microbiological evaluation

In the normal model group (NI) all results were negative in both of the experimental times. In the experimentally induced peri-implantitis models (I) all the swabs were positive. Indeed, at T1 the ASD + Ga showed a reduction of a viable bacteria as compared with ASD and CTR surfaces, whereas at T2 no differences among surfaces were detected (Fig. 3).

3.4 Histology

The histological analysis of the hematoxylin/eosin stained samples belonging to the normal group showed processes of primary bone formation starting from T1. Indeed, thin bone spicules branched from the pre-existing bone surface towards the implant interface, forming a thin longitudinal network of newly formed bone tissue that stabilizes the implant. This peri-implant bone had the typical morphology of a primary woven bone with big and round osteocyte lacunae and was more present and morphologically structured at the ASD and ASD + Ga interface than at CTR interface (Fig. 4). These findings were confirmed by Masson's trichrome analysis at T1, when a wide new deposition of osteoid matrix was detected for ASD and ASD + Ga, whereas it was scarce at CTR surface. Morphological differences also persisted at T2, when the histological observations showed a less compact and mature bone at the CTR interface and small areas of osteoid matrix only at ASD + Ga interface (Figs. 4, 6).

Clear differences in the histological findings between normal and experimentally induced peri-implantitis model

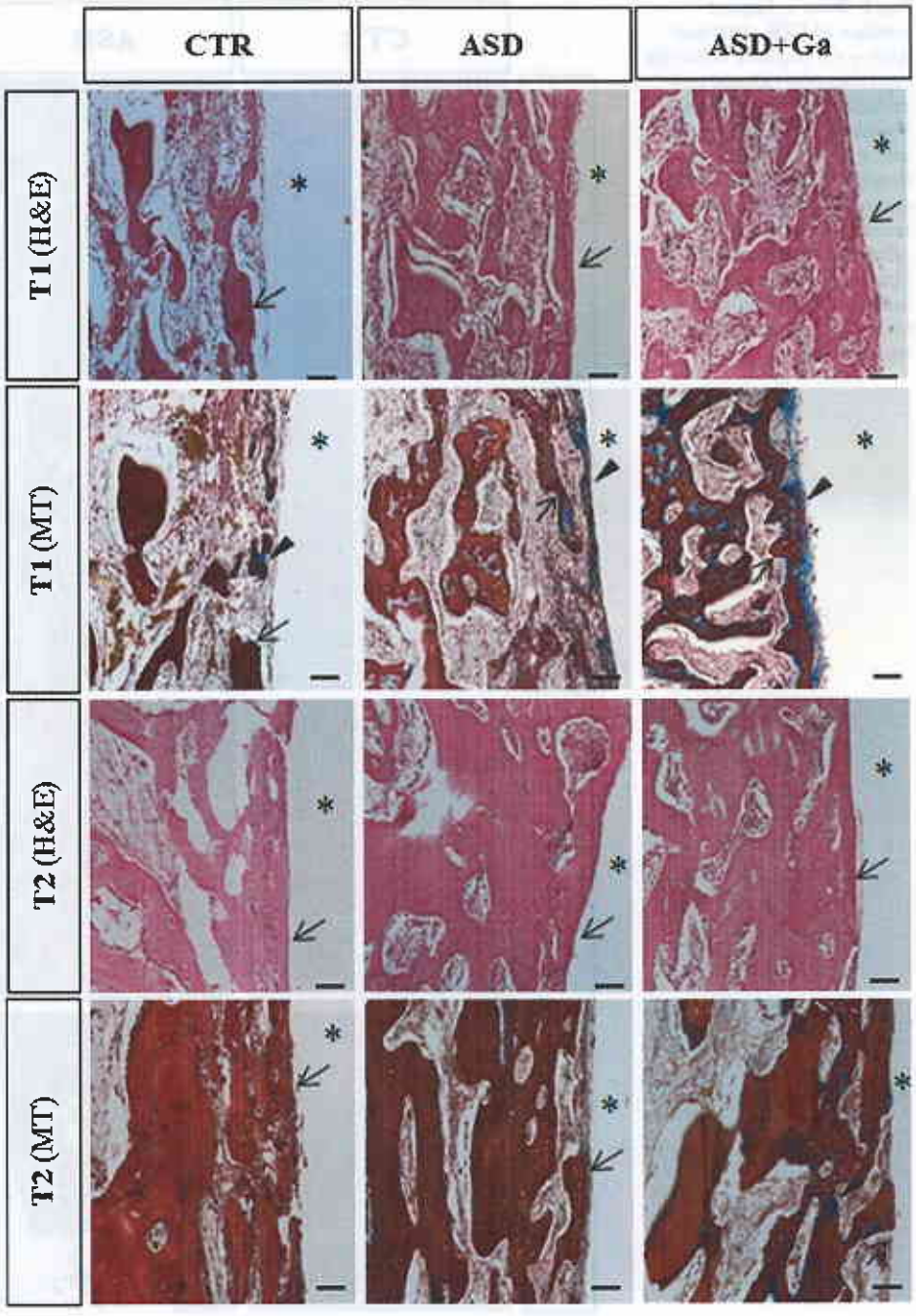

Fig. 4 Bone to implant interface of CTR, ASD and ASD + Ga implants within the normal model at T1 and T2. Marker = 100 μm. *Asterisk* indicates implant space. (H&E) Hematoxylin-eosin staining: the *arrows* indicate new bone. (MT) Masson's trichrome: the *arrows* indicate mineralized bone matrix, *arrowheads* indicate osteoid

were observed. Indeed in the latter, a typical acute suppurative inflammation characterized by a high recruitment of neutrophil granulocytes was observed at T1. As to CTR and ASD, the peri-implant tissue was extensively degenerated with osteolysis and foci of osteomyelitis, whereas in ASD + Ga the peri-implant tissue was more safeguarded. In that model, viable bone spicules at the interface could indeed still be observed. At T2, for all the surfaces, the histological observations showed a severely compromised bone tissue, that presented extensive areas of unviable bone tissue and necrosis (Figs. 5, 6).

The histological observations were also supported by the Gram stained sections, which showed a widespread bacterial colonization with presence of large bacterial colonies at the interface at T1 in the CTR samples, whereas a minor bacterial colonization was observed in ASD and ASD + Ga. At T2, large bacterial colonies were observed in all samples, even if they appeared slightly limited in ASD + Ga (Fig. 7).

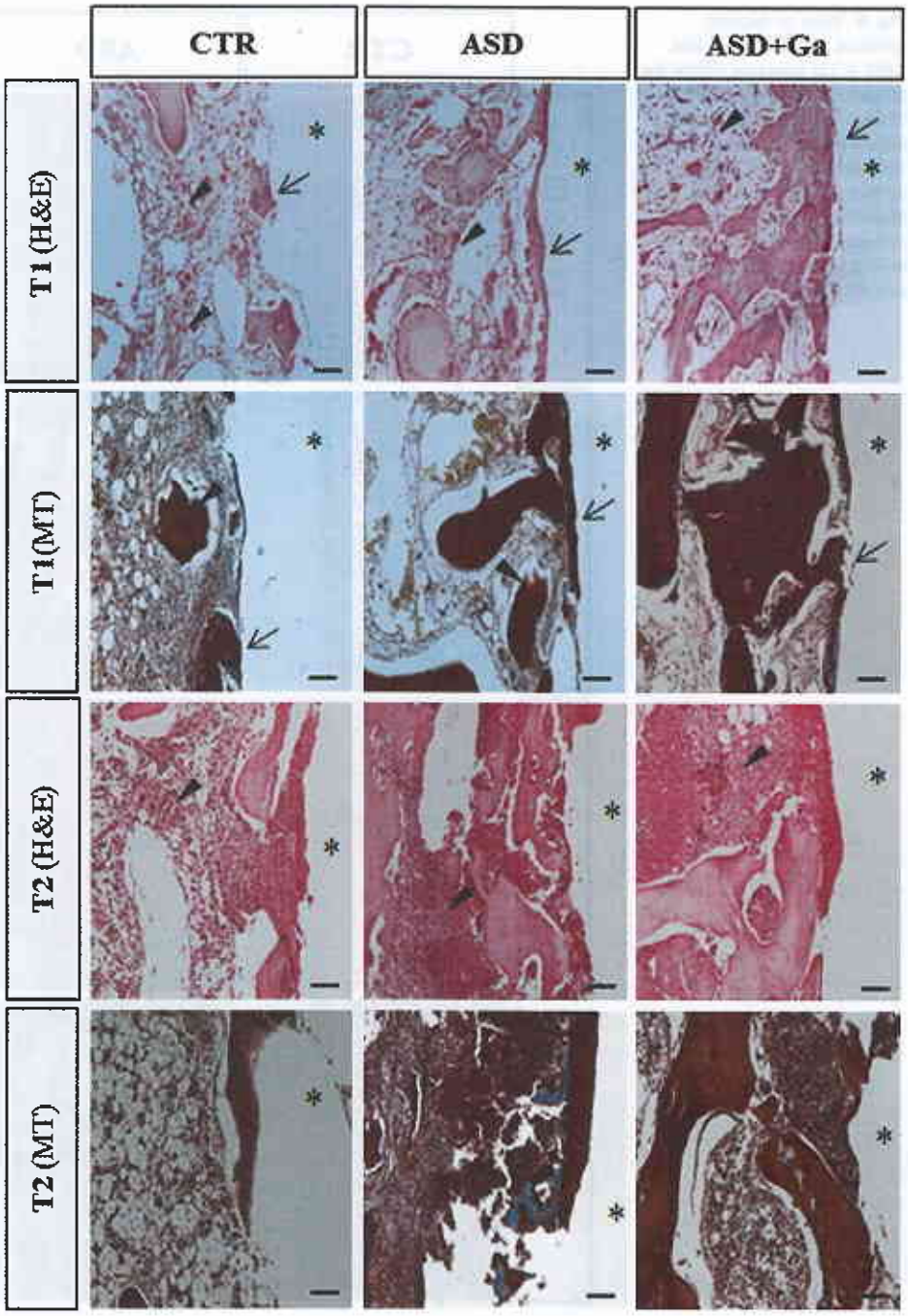

Fig. 5 Bone to implant interface of CTR, ASD and ASD + Ga implants within the experimentally induced peri-implantitis model at T1 and T2. Marker = 100 μm. *Asterisk* indicates implant space. (H&E) Hematoxylin-eosin staining: *arrow* indicates new bone; *arrowheads* indicate inflammatory infiltrate. (MT) Masson's trichrome: *arrows* indicate mineralized bone matrix; *arrowheads* indicate necrotic bone

3.5 Histomorphometry

The static histomorphometric parameters of bone to implant contact and bone volume were quantified by means of polarized light microscopy and represent the histological situation at the end of the experimental times (Fig. 8). The dynamic histomorphometric parameters mineralizing volume for CG and XO markers were quantified employing by means of fluorescence microscopy and represented the osteogenic activity at the marking time (Fig. 9). Histomorphometric data were reported in Table 1.

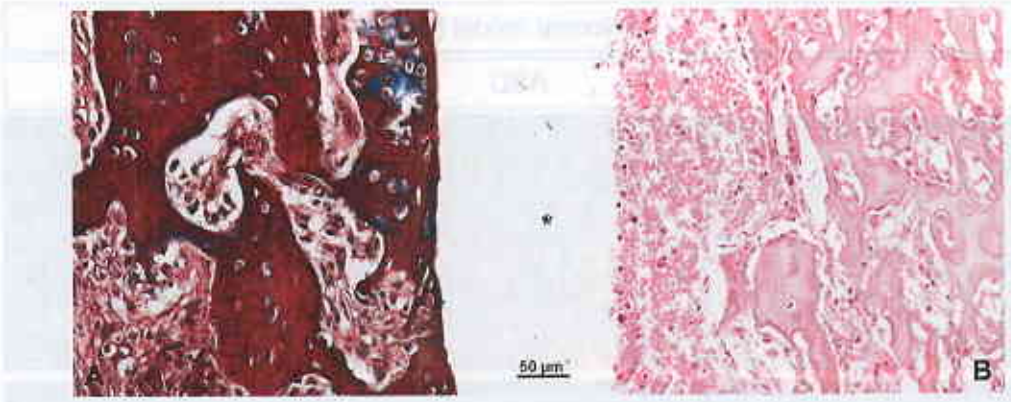

Fig. 6 Particular of ×20 magnification of **a** of the thin longitudinal network of newly formed bone at the ASD + Ga interface within the normal model at T1 stained with Masson trichrome and **b** acute suppurative inflammation at the interface characterized by a recruitment of neutrophil granulocytes at the interface of ASD + Ga at T1 stained with Hematoxylin and Eosin. *Asterisk* indicates implant space

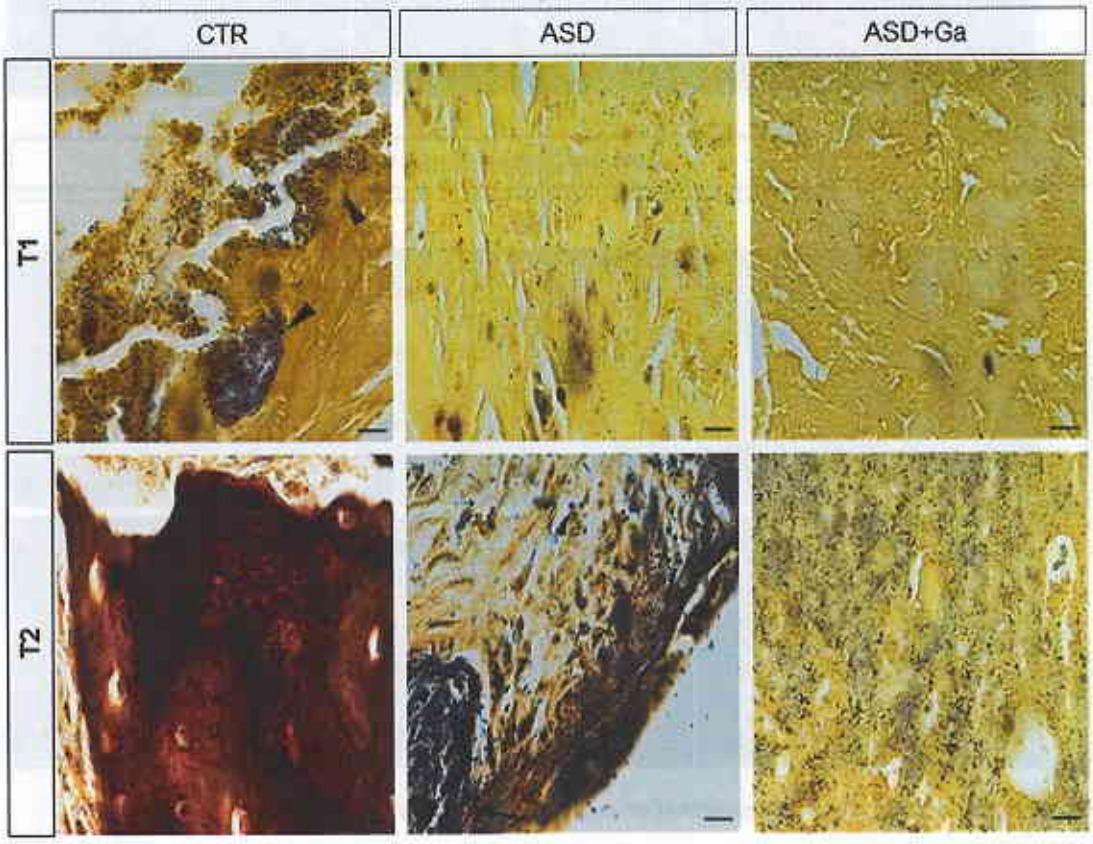

Fig. 7 Gram staining of peri-implant tissue in the experimentally induced peri-implantitis model at T1 and T2. Marker = 10 µm. The colonization of *Staphylococcus aureus* (gram +) is *purple* stained (Color figure online)

3.6 Bone to implant contact

In the normal model, at T1 the surfaces ASD and ASD + Ga showed a greater bone to implant contact compared with CTR ($P < 0.05$). At T2, the BIC is increased compared with T1 and was greater in ASD and ASD + Ga than in CTR, but with a statistical significance only for ASD ($P < 0.05$) (Fig. 10a). The same trend observed in the normal model was maintained in the experimentally induced peri-implantitis model. At T1

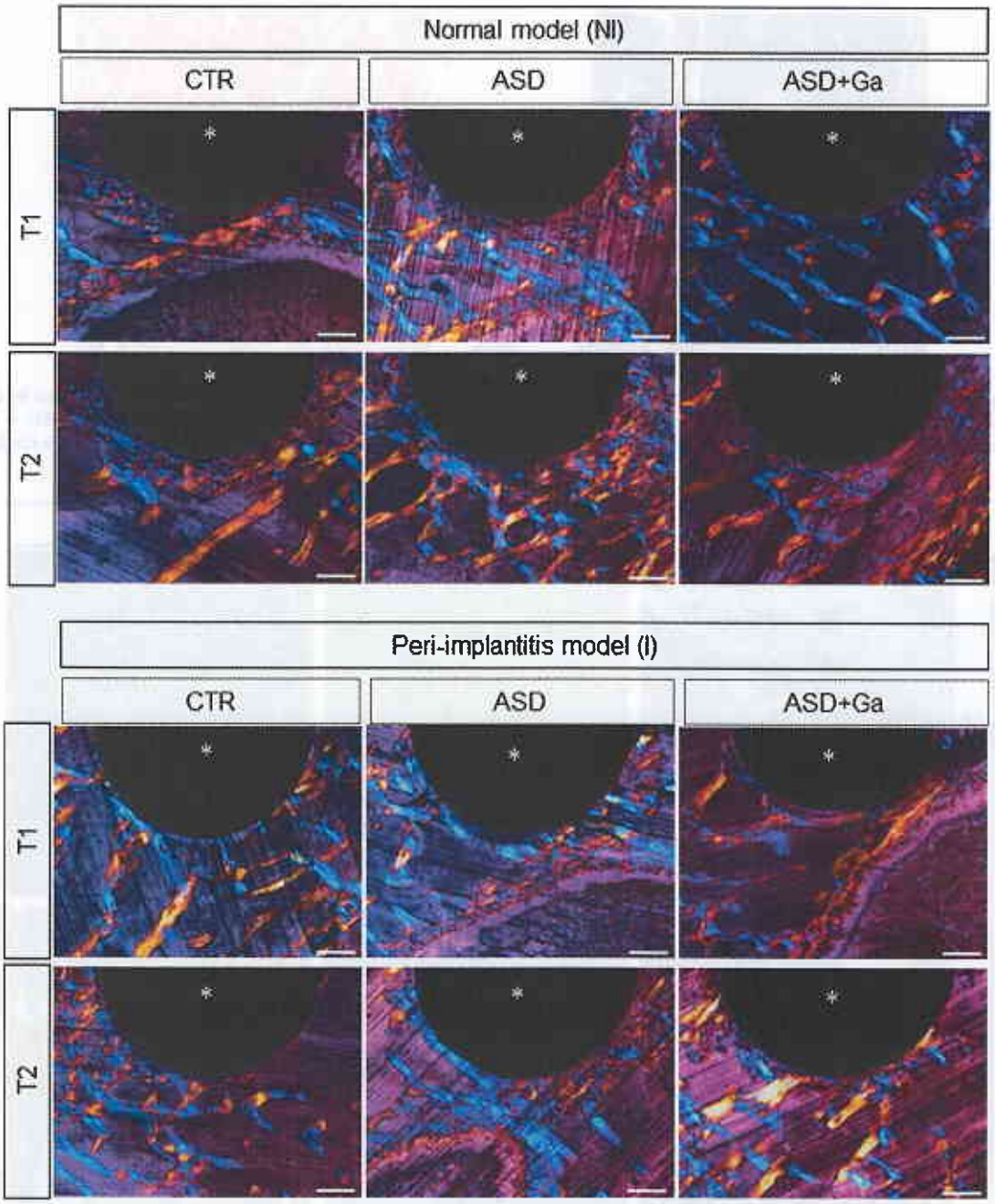

Fig. 8 Polarized light microscopy for the determination of the static histomorphometric parameters

the bone to implant contact resulted higher in ASD and significantly higher in ASD + Ga ($P < 0.05$) as compared with CTR. Finally, BIC was significantly higher at T2 both in ASD ($P < 0.05$) and ASD + Ga ($P < 0.001$) than CTR (Fig. 10b).

3.7 Bone volume

In the normal model, BV at T1 was significantly higher in the ASD and ASD + Ga compared with CTR ($P < 0.05$). At T2, BV increased due to bone deposition activity and the same trend

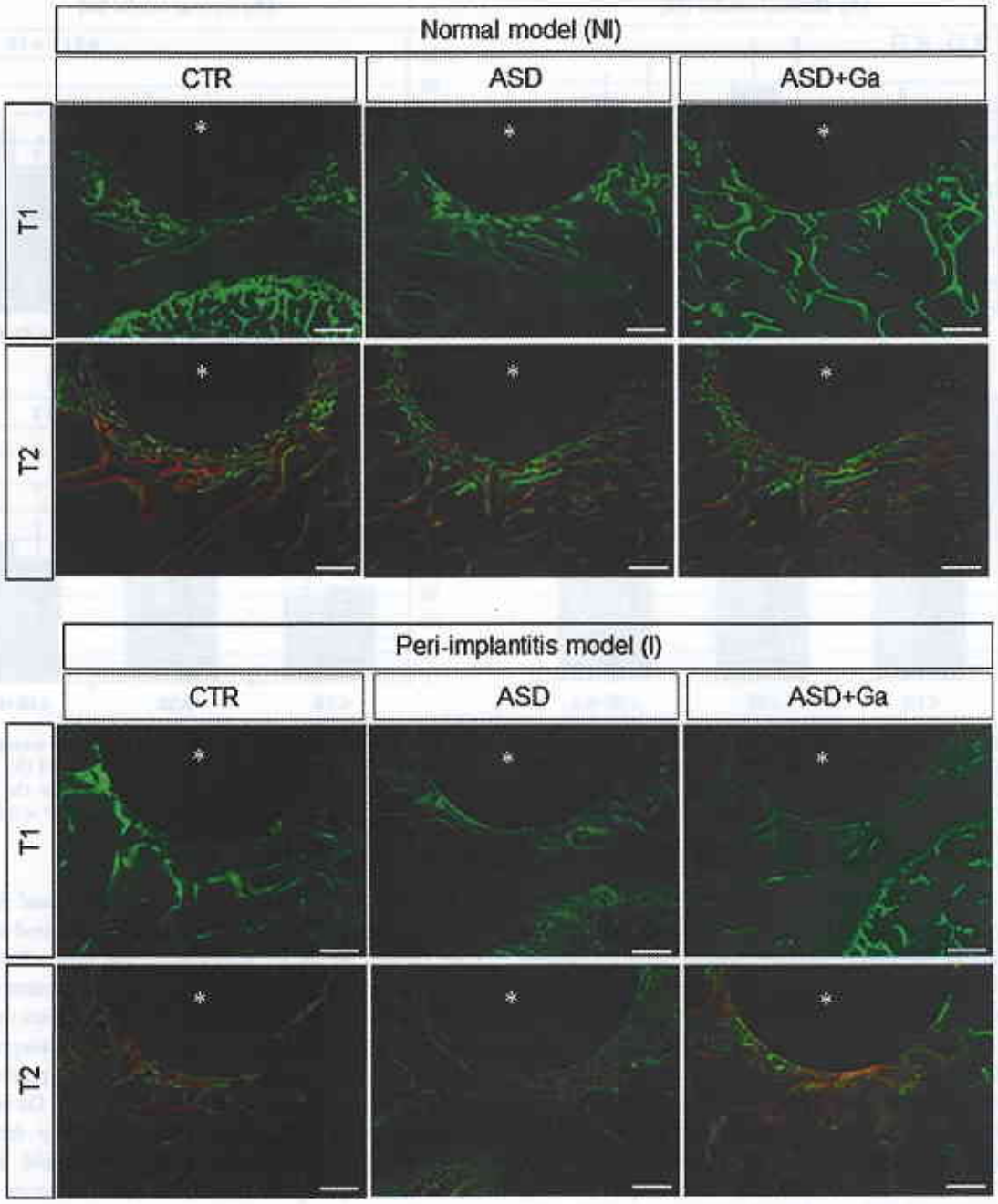

Fig. 9 Fluorescence microscopy for the determination of the dynamic histomorphometric parameters

was maintained, though with no statistical significance (Fig. 11a). Regarding the experimentally induced peri-implantitis model, the same trend was maintained at both the experimental times, but a decrease in BV values was found. No statistically significant differences among surfaces were detectable at T1, whereas at T2, BV was significantly higher in ASD + Ga than in CTR ($P < 0.05$) (Fig. 11b).

3.8 Mineralizing volume

In the normal model at T1, the surfaces ASD and ASD + Ga were higher when compared to the CTR, though with no statistical significance. At T2, the MV-CG decreased and resulted similar for the three surfaces, due to the bone remodeling activity that had occurred between the

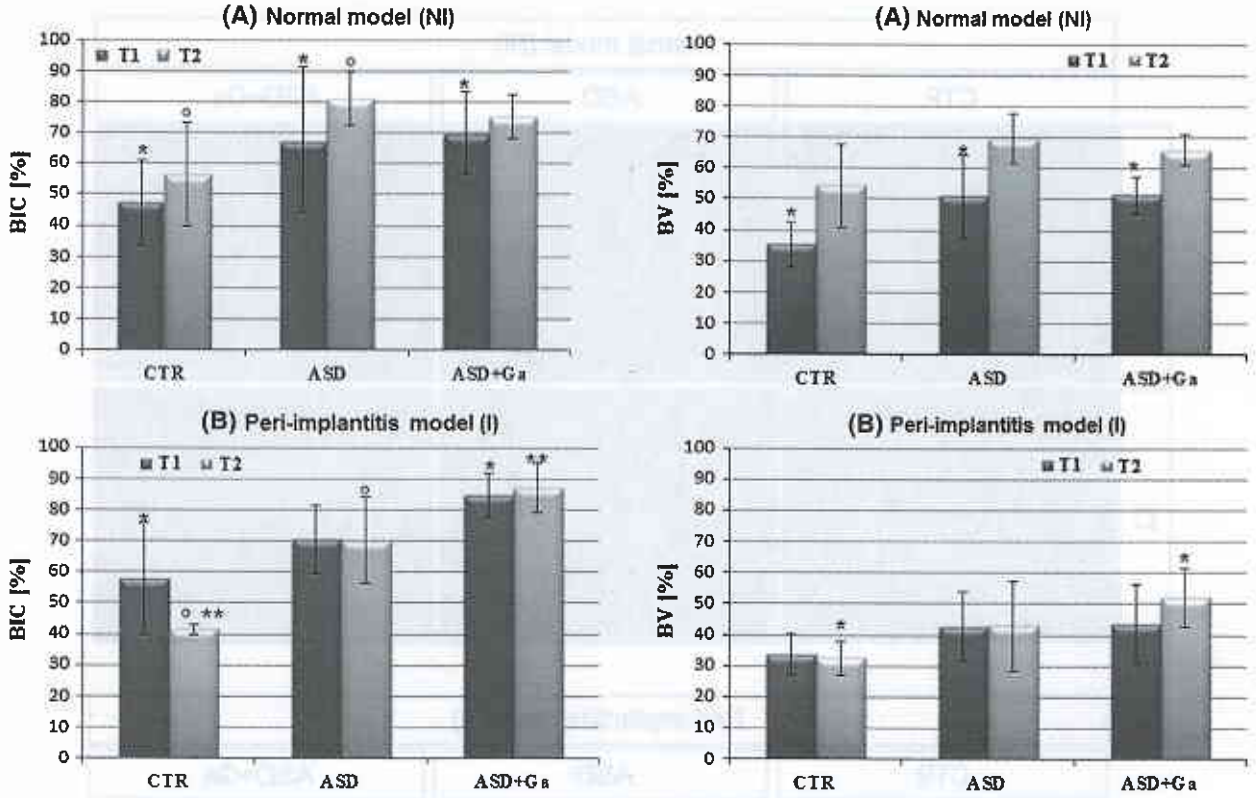

Fig. 10 Bone to implant contact (BIC) at T1 and T2 for the normal model (**a**) and experimentally induced peri-implantitis model (**b**). **a** *CTR (NI-T1) versus ASD (NI-T1) and versus ASD + Ga (NI-T1) $P < 0.05$; ° CTR (NI-T2) versus ASD (NI-T2) $P < 0.05$. **b** *CTR (I-T1) versus ASD (I-T1) $P < 0.05$; ° CTR (I-T2) versus ASD (I-T2) $P < 0.05$; ** CTR (I-T2) versus ASD + Ga (I-T2) $P < 0.001$

Fig. 11 Bone volume (BV) at T1 and T2 for the normal model (**a**) and experimentally induced peri-implantitis model (**b**). **a** *CTR (NI-T1) versus ASD (NI-T1) and versus ASD + Ga (NI-T1) $P < 0.05$. **b** * CTR (I-T2) versus ASD + Ga (I-T2) $P < 0.05$

marking period and the end of experimental time (Fig. 12a). In the experimentally induced peri-implantitis model, MV-CG for the ASD + Ga surface was significantly higher compared with ASD and CTR ($P < 0.001$). At T2, the bone remodeling activity influenced the outcome of MV-CG, leading to lower and similar values of this parameter in all surfaces (Fig. 12b). Considering the administration timing of XO marker, the parameter MV-XO could be evaluated only at T2. All the tested surfaces showed a similar values of MV-XO; in the experimentally induced peri-implantitis model a decrease in the osteogenic activity was observed for all samples when compared with the homologous in the normal model.

4 Discussion

In the normal model, the osteogenic response of ASD and ASD + Ga surfaces showed a greater new bone deposition than CTR at the first experimental time, as documented by the higher bone mineralizing volume that is expressed in higher bone implant contact and bone volume compared with the CTR surface. At the second experimental time, all materials show similar osseointegration parameters. Importantly, the gallium functionalization of the ASD + Ga surface treatment does not impair the speed and quality of osseointegration as compared to ASD treatment. The obtained data pointed out a more rapid primary fixation in ASD and ASD + Ga implants, compared with CTR. This represents a key factor for stable and durable osseointegration, as could improve antibacterial activity. Indeed, if the tissue achieves a good integration as fast as possible, the surface is defended and is less available for bacterial colonization.

These findings agree with previous studies, the ASD surfaces showed a high mineralization potential both in vitro and in vivo, representing an attractive surface to osteoblast adhesion, spreading and differentiation. Moreover, in vivo studies showed excellent bone growth in direct contact with titanium surface [42–47].

As to the effects of gallium on bone metabolism, studies showed the inhibitory effect of Ga on osteoclastic

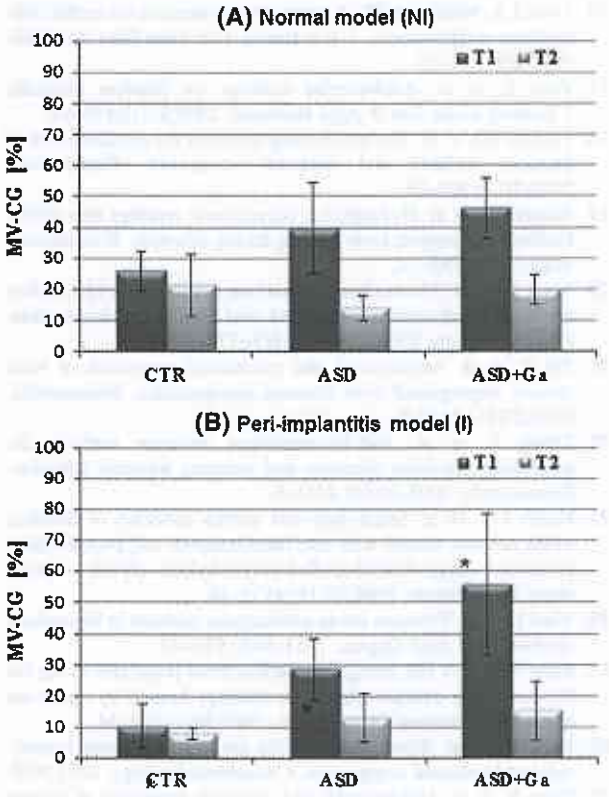

Fig. 12 Mineralizing volume for the CG marker (MV-CG) at T1 and T2 for the normal model (**a**) and experimentally induced peri-implantitis model (**b**). **b** CTR (I-T1) versus ASD (I-T1) and versus ASD + Ga (I-T1) $P < 0.001$

resorption activity [48–54] and it was demonstrated that this is not associated with a reduction of multinucleated osteoclast-like cells, suggesting that Ga does not interfere with the recruitment or the differentiation of bone resorbing cells. The antiosteoclastic properties of gallium involve the downregulation of NFATc1, a master regulator of RANK-induced osteoclastic differentiation [48, 55] and moreover a direct inhibition of the proteasome activity [56]. Regarding the effects of gallium on osteoblasts, it is reported that the Ga treatment failed to affect the viability, the proliferation and the alkaline phosphatase activity [37] in vitro. In addition, neither was the expression of osteoblastic marker genes modified, nor was the bone mineral density [55]. In vitro activity of gallium against important human pathogens such as *M. avis, P. aeruginosa, R. equi, Salmonella* and staphylococci was demonstrated [32, 33, 57]. Its ability to inhibit the growth of staphylococci is of great interest as these pathogens are now a significant source of human and veterinary infections [58]. With the experimentally induced peri-implantitis model we had evaluated the osteoprotective potential and the antibacterial effect of the tested surfaces. The obtained results at the first experimental time (1 week) showed a better osseointegration of the surfaces ASD and ASD + Ga compared with CTR, with statistical significance limited to ASD + Ga for parameters BIC and MV-CG. At the second experimental time (2 weeks), an ASD + Ga surface-induced protective effect was testified by a lower tissue erosion, with significantly higher BV than in CTR and higher than ASD. A more preserved peri-implant tissue from bone degeneration for ADS + Ga implants was also confirmed by histology.

The surface induced effects on infection at the first experimental time consist in infection containment given by ASD + Ga compared to other surfaces and an evident inhibition of bacterial tissue colonization. The effects induced on infection by the surface at the first experimental time consisted in an infection containment by ASD + Ga in comparison with other surfaces and a marked inhibition of bacterial tissue colonization. Such features were proved by both microbiological swab and Gram staining performed on peri-implant tissue. At the second time point the bacterial colonisation is so widespread as not be controllable by the only antibacterial activity of the surface without antibiotic treatment. Our results corroborate previous findings available in the literature about the effectiveness of gallium compounds in bacterial inhibition [35, 59, 60]. The evaluation of these data should take into account that the inoculation concentration chosen for the development of the infected model is higher than that occurring in natural conditions [61], and that no antibiotic administration was carried out. Al tempo 2 no differenze per eccesso di infezione batterica (non controllabile senza terapia antibiotica) Moreover it must be considered that the acidic environment may promote Ga elution from ASD samples, inducing an higher release rates compared to neutral environment [62].

In the experimentally induced peri-implantitis model ASD surface turned out to be significantly better than CTR surface. This may be due to the presence of anatase within the surface. It was indeed reported in the literature that anatase could confer a slight antibacterial activity to all ASD coatings, since it plays an important role in decreasing bacterial adhesion and proliferation.

In the experimentally induced peri-implantitis model ASD surface turned out to be significantly better than CTR surface. This may be due to the peculiar oxide characteristics as described and reported elsewhere [63].

5 Conclusion

This study presents the first evidence of the effects of Gallium doped titanium surface on the osteogenic response and osseointegration. Regarding the osteointegration

process, the obtained data point out a more rapid primary fixation in ASD and ASD + Ga implants, compared with CTR surface. Regarding the antibacterial properties, the ASD + Ga surface shows osteoprotective action on bone peri-implant tissue in vivo at both the considered experimental time considered as well as an antibacterial effect within the first considered time point.

Acknowledgments The authors would like to thank Eurocoating S.p.A. for their liberal donation that contributed the funding of this study. Furthermore, they declare no conflict of interest.

References

1. Mangram AJ, et al. Guideline for prevention of surgical site infection, 1999. Centers for Disease Control and Prevention (CDC) Hospital Infection Control Practices Advisory Committee. Am J Infect Control. 1999;27(2):97–132 **quiz 133–134; discussion 96**.
2. Hayes G, Moens N, Gibson T. A review of local antibiotic implants and applications to veterinary orthopaedic surgery. Vet Comp Orthop Traumatol. 2013;26(4):251–9.
3. Gristina A. Biomaterial-centered infection: microbial adhesion versus tissue integration. Clin Orthop Relat Res. 1987;2004(427):4–12.
4. Katsikogianni M, Missirlis YF. Concise review of mechanisms of bacterial adhesion to biomaterials and of techniques used in estimating bacteria-material interactions. Eur Cell Mater. 2004;8:37–57.
5. Campoccia D, Montanaro L, Arciola CR. The significance of infection related to orthopedic devices and issues of antibiotic resistance. Biomaterials. 2006;27(11):2331–9.
6. Gristina AG. Implant failure and the immuno-incompetent fibro-inflammatory zone. Clin Orthop Relat Res. 1994;298:106–18.
7. Arciola CR, et al. Interactions of staphylococci with osteoblasts and phagocytes in the pathogenesis of implant-associated osteomyelitis. Int J Artif Organs. 2012;35(10):713–26.
8. Hudson MC, Ramp WK, Frankenburg KP. Staphylococcus aureus adhesion to bone matrix and bone-associated biomaterials. FEMS Microbiol Lett. 1999;173(2):279–84.
9. Del Pozo JL, Patel R. Clinical practice. Infection associated with prosthetic joints. N Engl J Med. 2009;361(8):787–94.
10. Wininger DA, Fass RJ. Antibiotic-impregnated cement and beads for orthopedic infections. Antimicrob Agents Chemother. 1996;40(12):2675–9.
11. Ethell MT, et al. In vitro elution of gentamicin, amikacin, and ceftiofur from polymethylmethacrylate and hydroxyapatite cement. Vet Surg. 2000;29(5):375–82.
12. Andersson RE, et al. Local administration of antibiotics by gentamicin-collagen sponge does not improve wound healing or reduce recurrence rate after pilonidal excision with primary suture: a prospective randomized controlled trial. World J Surg. 2010;34(12):3042–8.
13. Lapid O. Use of gentamicin collagen sponges for the treatment of periprosthetic breast implant infection. J Plast Reconstr Aesthet Surg. 2011;64(12):e313–6.
14. Lewis CS, et al. Local antibiotic delivery with demineralized bone matrix. Cell Tissue Bank. 2012;13(1):119–27.
15. Diefenbeck M, Mückley T, Hofmann GO. Prophylaxis and treatment of implant-related infections by local application of antibiotics. Injury. 2006;37(Suppl 2):S95–104.
16. Cohn LA, Middleton JR. A veterinary perspective on methicillin-resistant staphylococci. J Vet Emerg Crit Care (San Antonio). 2010;20(1):31–45.
17. Zhao L, et al. Antibacterial coatings on titanium implants. J Biomed Mater Res B Appl Biomater. 2009;91(1):470–80.
18. Puckett SD, et al. The relationship between the nanostructure of titanium surfaces and bacterial attachment. Biomaterials. 2010;31(4):706–13.
19. Schaer TP, et al. Hydrophobic polycationic coatings that inhibit biofilms and support bone healing during infection. Biomaterials. 2012;33(5):1245–54.
20. Visai L, et al. Electrochemical surface modification of titanium for implant abutments can affect oral bacteria contamination. J Appl Biomater Biomech. 2008;6(3):170–7.
21. Shi Z, et al. Antibacterial and mechanical properties of bone cement impregnated with chitosan nanoparticles. Biomaterials. 2006;27(11):2440–9.
22. Zhang F, et al. Silk-functionalized titanium surfaces for enhancing osteoblast functions and reducing bacterial adhesion. Biomaterials. 2008;29(36):4751–9.
23. Harris LG, et al. Staphylococcus aureus adhesion to titanium oxide surfaces coated with non-functionalized and peptide-functionalized poly(L-lysine)-grafted-poly(ethylene glycol) copolymers. Biomaterials. 2004;25(18):4135–48.
24. Visai L, et al. Titanium oxide antibacterial surfaces in biomedical devices. Int J Artif Organs. 2011;34(9):929–46.
25. Song WH, Ryu HS, Hong SH. Antibacterial properties of Ag (or Pt)-containing calcium phosphate coatings formed by micro-arc oxidation. J Biomed Mater Res A. 2009;88(1):246–54.
26. Lara HH, et al. Silver nanoparticles are broad-spectrum bactericidal and virucidal compounds. J Nanobiotechnology. 2011;9:30.
27. Chen Y, et al. Anti-bacterial and cytotoxic properties of plasma sprayed silver-containing HA coatings. J Mater Sci Mater Med. 2008;19(12):3603–9.
28. Fiedler J, et al. Copper and silver ion implantation of aluminium oxide-blasted titanium surfaces: proliferative response of osteoblasts and antibacterial effects. Int J Artif Organs. 2011;34(9):882–8.
29. Zheng Y, et al. Antimicrobial and osteogenic effect of Ag-implanted titanium with a nanostructured surface. Int J Nanomedicine. 2012;7:875–84.
30. Lansdown AB. Silver in health care: antimicrobial effects and safety in use. Curr Probl Dermatol. 2006;33:17–34.
31. Bernstein LR. Mechanisms of therapeutic activity for gallium. Pharmacol Rev. 1998;50(4):665–82.
32. Olakanmi O, et al. Polyvalent cationic metals induce the rate of transferrin-independent iron acquisition by HL-60 cells. J Biol Chem. 1997;272(5):2599–606.
33. Nerren JR, et al. Evaluation of the effect of gallium maltolate on fecal Salmonella shedding in cattle. J Food Prot. 2011;74(4):524–30.
34. Cochis A, et al. Biofilm formation on titanium implants counteracted by grafting gallium and silver ions. J Biomed Mater Res A. 2015;103(3):1176–87.
35. Kaneko Y, et al. The transition metal gallium disrupts *Pseudomonas aeruginosa* iron metabolism and has antimicrobial and antibiofilm activity. J Clin Invest. 2007;117(4):877–88.
36. Niesvizky R. Gallium nitrate in multiple myeloma: prolonged survival in a cohort of patients with advanced-stage disease. Semin Oncol. 2003;30(2 Suppl 5):20–4.
37. Verron E, et al. Gallium modulates osteoclastic bone resorption in vitro without affecting osteoblasts. Br J Pharmacol. 2010;159(8):1681–92.
38. Chai H, et al. Antibacterial effect of 317L stainless steel contained copper in prevention of implant-related infection in vitro and in vivo. J Mater Sci Mater Med. 2011;22(11):2525–35.

39. Della Valle C, et al. A novel silicon-based electrochemical treatment to improve osteointegration of titanium implants. J Appl Biomater Funct Mater. 2013;11(2): e106–16.
40. van Gaalen SM, et al. Use of fluorochrome labels in in vivo bone tissue engineering research. Tissue Eng Part B Rev. 2010; 16(2):209–17.
41. Dempster DW, et al. Standardized nomenclature, symbols, and units for bone histomorphometry: a 2012 update of the report of the ASBMR Histomorphometry Nomenclature Committee. J Bone Miner Res. 2013;28(1):1–16.
42. Ravanetti F, et al. In vitro cellular response and in vivo primary osteointegration of electrochemically modified titanium, in Acta Biomater. 2010, 2009 Acta Materialia Inc. Published by Elsevier Ltd: England. p. 1014-24.
43. Chiesa R, et al. In vitro and in vivo performance of a novel surface treatment to enhance osseointegration of endosseous implants. Oral Surg Oral Med Oral Pathol Oral Radiol Endod. 2007;103(6):745–56.
44. Giavaresi G, et al. Mechanical and histomorphometric evaluations of titanium implants with different surface treatments inserted in sheep cortical bone. Biomaterials. 2003;24(9):1583–94.
45. Giavaresi G, et al. A novel multiphase anodic spark deposition coating for the improvement of orthopedic implant osseointegration: an experimental study in cortical bone of sheep. J Biomed Mater Res A. 2008;85(4):1022–31.
46. Giavaresi G, et al. Histomorphometric and microhardness assessments of sheep cortical bone surrounding titanium implants with different surface treatments. J Biomed Mater Res A. 2003;67(1):112–20.
47. Giavaresi G, et al. Effect of a multiphasic anodic spark deposition coating on the improvement of implant osseointegration in the osteopenic trabecular bone of sheep. Int J Oral Maxillofac Implants. 2008;23(4):659–68.
48. Verron E, Bouler JM, Scimeca JC. Gallium as a potential candidate for treatment of osteoporosis. Drug Discov Today. 2012;17(19–20):1127–32.
49. Bockman R. The effects of gallium nitrate on bone resorption. Semin Oncol. 2003;30(2 Suppl 5):5–12.
50. Hall TJ, Chambers TJ. Gallium inhibits bone resorption by a direct effect on osteoclasts. Bone Miner. 1990;8(3):211–6.
51. Liewehr FR, et al. Effect of bisphosphonates and gallium on dentin resorption in vitro. Endod Dent Traumatol. 1995;11(1): 20–6.
52. Lakatos P, Mong S, Stern PH. Gallium nitrate inhibits bone resorption and collagen synthesis in neonatal mouse calvariae. J Bone Miner Res. 1991;6(10):1121–6.
53. Blair HC, et al. Reversible inhibition of osteoclastic activity by bone-bound gallium (III). J Cell Biochem. 1992;48(4):401–10.
54. Shaini FJ, et al. In vitro evaluation of the effect of freshly mixed amalgam and gallium-based alloy on the viability of primary periosteal and osteoblast cell cultures. Biomaterials. 2000;21(2): 113–9.
55. Jenis LG, et al. Effect of gallium nitrate in vitro and in normal rats. J Cell Biochem. 1993;52(3):330–6.
56. Verron E, et al. Molecular effects of gallium on osteoclastic differentiation of mouse and human monocytes. Biochem Pharmacol. 2012;83(5):671–9.
57. DeLeon K, et al. Gallium maltolate treatment eradicates *Pseudomonas aeruginosa* infection in thermally injured mice. Antimicrob Agents Chemother. 2009;53(4):1331–7.
58. Arnold CE, et al. Antimicrobial activity of gallium maltolate against *Staphylococcus aureus* and methicillin-resistant *S. aureus* and *Staphylococcus pseudintermedius*: an in vitro study. Vet Microbiol. 2012;155(2–4):389–94.
59. Valappil SP, et al. Effect of novel antibacterial gallium-carboxymethyl cellulose on *Pseudomonas aeruginosa*. Dalton Trans. 2013;42(5):1778–86.
60. Valappil SP, et al. Role of gallium and silver from phosphate-based glasses on in vitro dual species oral biofilm models of *Porphyromonas gingivalis* and *Streptococcus gordonii*. Acta Biomater. 2012;8(5):1957–65.
61. Patel M, et al. Animal models for the study of osteomyelitis. Semin Plast Surg. 2009;23(2):148–54.
62. Cèsar LC. Long-term stability assessment of antibacterial tratment of titanium., in Department of Chemistry, Materials and Materials Engineering "G. Natta". 2014, Politecnico di Milano: Master Thesis.
63. Cochis A, et al. The effect of silver or gallium doped titanium against the multidrug resistant *Acinetobacter baumannii*. Biomaterials. 2016. doi: 10.1016/j.biomaterials.2015.11.042